TENSION FRACTURE OF LAMINATES FOR TRANSPORT FUSELAGE PART II: LARGE NOTCHES[1]

T. H. Walker, L. B. Ilcewicz
Boeing Commercial Airplane Group

D. R. Polland
Boeing Defense and Space Group

C. C. Poe, Jr.
NASA Langley Research Center

ABSTRACT

Tests were conducted on over 200 center-crack specimens to evaluate (a) the tension-fracture performance of candidate materials and laminates for commercial fuselage applications and (b) the accuracy of several failure criteria in predicting response. Crack lengths of up to 12 inches were considered. Other variables included fiber/matrix combination, layup, lamination manufacturing process, and intraply hybridization. Laminates fabricated using the automated tow-placement process provided significantly higher tension-fracture strengths than nominally identical tape laminates. This confirmed earlier findings for other layups, and possibly relates to a reduced stress concentration resulting from a larger scale of repeatable material inhomogeneity in the tow-placed laminates. Changes in material and layup result in a trade-off between small-notch and large-notch strengths. Toughened resins and 0°-dominate layups result in higher small-notch strengths but lower large-notch strengths than brittle resins, 90°- and 45°-dominated layups, and intraply S2-glass hybrid material forms. Test results indicate that strength-prediction methods that allow for a reduced order singularity of the crack-tip stress field are more successful at predicting failure over a range of notch sizes than those relying on the classical square-root singularity. The order of singularity required to accurately predict large-notch strength from small-notch data was affected by both material and layup. Measured crack-tip strain distributions were generally higher than those predicted using classical methods. Traditional methods of correcting for finite specimen width were found to be lacking, confirming earlier findings with other specimen geometries. Fracture tests of two stiffened panels, identical except for differing materials, with severed central stiffeners resulted in nearly identical damage progression and failure sequences. Strain-softening laws implemented within finite element models appear attractive to account for load redistribution in configured structure due to damage-induced crack tip softening.

---

[1] This work was funded by Contract NAS1-18889, under the direction of J. G. Davis and W. T. Freeman of NASA Langley Research Center

INTRODUCTION

Boeing's program for Advanced Technology Composite Aircraft Structure (ATCAS) is studying manufacturing and performance issues associated with a wide body commercial transport fuselage (Ref. 1). Tension damage tolerance and pressure containment are major technical issues to solve for fuselage structures. Although composites are generally thought to have excellent tension properties, only limited data exists on the performance of configured composite shell structures with large through-penetrating damage and are subjected to combined load conditions, including pressure. A collaborative effort between Boeing and NASA is committed to collecting a database and solving the technical challenges associated with composite fuselage damage tolerance.

The tension fracture studies for the crown region include seven types of tests, as shown in Figure 1. The upper row illustrates uniaxial tension tests, while the lower row contains those for biaxial tension. The numbers shown parenthetically are the specimen quantities. Significant progress has been made towards completion of the testing. As of June 1992, the tests remaining include several flat tear-strap panels and the curved stiffened panels. The focus of this paper is the coupon and large unstiffened panel tests, but the results obtained from the large stiffened panel tests conducted during May of 1992 are also briefly discussed. A discussion of the curved tear strap panel test, also conducted during May of 1992, and the plans for the curved stiffened panels are contained in Reference 2.

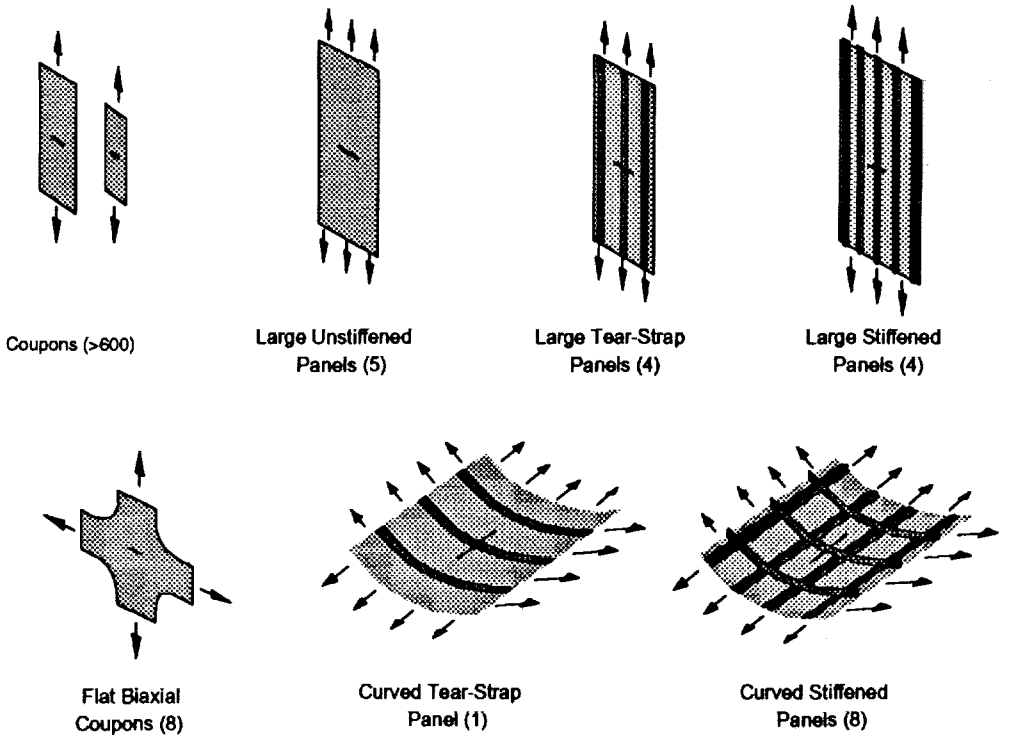

Figure 1. ATCAS tension fracture testing.

This paper is the second in a series on ATCAS tension fracture studies. The first paper (Ref. 3) discussed several significant experimental and theoretical findings. Experimental

results were based on 430 uniaxial tension tests of specimens with notch sizes between 0.25 and 5.0 inches. The most important findings are summarized below.

1. Laminates fabricated using the advanced tow-placement process were found to have significantly higher tension fracture performance than identical laminates that were fabricated by hand layup from nominally identical prepreg tape (i.e., the same fiber, fiber bundle size, resin, resin content, areal weight and ply thickness). This improvement was hypothesized to relate to a larger scale of repeatable material inhomogeneity in the tow-placed laminates.

2. Brittle-resin laminates tested with sharp penetrations created by an impact event and machined slits of comparable dimension displayed similar strengths for the thinnest laminates tested (t = 0.074 in.). For thicker brittle-resin laminates (t = 0.118 in.), the machined slit resulted in approximately 25% lower strengths than the through-penetration. For toughened-resin laminates, the through-penetration specimens provided 22% lower strengths than the machined slit coupons.

3. Classical finite width correction factors did not properly account for the differences between notched strengths of specimens with width-to-notch-length ratios ($W/2a$) of 2 and 4. This was found to be true for a range of fibers, matrices, fabrication techniques and layups.

4. Intraply hybridization with higher strain fibers reduced the sensitivity of a material to changes in notch length. Significant precatastrophic damage was observed in such laminates.

5. Increased matrix toughness was found to increase the sensitivity of the material to changes in notch size. A representative toughened-matrix system, IM7[2]/8551-7[3], was found to have 35% higher strength at 0.25 in. notch sizes than a brittle-matrix system with a nearly identical fiber, IM6[4]/937A[5]. However, the advantage had turned into a 7% disadvantage for 2.5 in. notches. This behavior was suggested to relate to reduced matrix damage in the vicinity of the notch tip for the toughened-matrix material, which in turn limits stress relief.

6. Layup was found to affect notch strength for a single notch size and the sensitivity to changes in notch length.

7. Classical fracture toughness values obtained from experimental data increased with increasing notch size.

---

[2] IM7 is a graphite fiber system produced by Hercules, Inc.

[3] 8551-7 is a resin system produced by Hercules, Inc.

[4] IM6 is a graphite fiber system produced by Hercules, Inc.

[5] 937A is a resin system produced by ICI/Fiberite

8. Four failure criteria were evaluated for accuracy in predicting the effect of notch size. Failure criteria that used a classical crack-tip stress-field singularity of 0.5 were less successful in predicting the test results than methods using 0.3.

Significant efforts have been conducted in understanding the damage tolerance of stiffened metallic structure (e.g., Ref. 4, 5). Competing failure mechanisms in such structure are skin fracture, stiffener strength, and rivet yielding. Consideration of the inelastic behavior of the material has been found to be important in properly predicting the interaction between these competing failure mechanisms. It was also found that stiffener bending is an important aspect to predicting load redistribution and stiffener strength. Similar failure mechanisms exist for composite structure with bonded stiffening elements. Skin fracture and stiffener strength both remain important, and delamination of the stiffener from the skin replaces rivet yielding, since both control the local load transfer into the stiffening element in their respective configurations. It is likely, then, that local damage growth in composite materials is important in predicting strengths of configured composite structure since it is the mechanism by which composite materials exhibit significant inelastic behavior. Additional discussions of failure mechanisms for configured composite structure are contained in Reference 1.

EXPERIMENTS

Test Matrix

Nearly two-hundred coupons and five large flat unstiffened panels have been tested since the initial paper on ATCAS tension fracture activities (Ref. 3). A summary of the test specimen configurations and quantities are contained in Figure 2. Laminates were made of combinations of three fiber (AS4[6], S2-Glass[7], IM7) and two resin (938[8], 8551-7) types. The first two materials indicated in the figure, AS4/938 tape and AS4/938 tow, provided a direct comparison of laminates fabricated using the tow-placement and hand layup processes. The IM7/8551-7 system represented the toughened-resin class of materials. Intraply hybrid materials, consisting of alternating bands of differing fibers within some or all of the laminate plies as shown schematically in Figure 3, were included to further evaluate their attractive fracture characteristics.

Several laminates representative of crown applications were considered, including aft (Crown3, 2/4/6, 4/4/4) and forward (Crown4) portions of the ATCAS study section. Most laminates were tested in the directions corresponding to both the axial and hoop directions of the fuselage.

---

[6] AS4 is a graphite fiber system produced by Hercules, Inc.

[7] S2 is a glass fiber system produced by Owens-Corning Fiberglas, Corp.

[8] 938 is a resin system produced by ICI/Fiberite

	Notch Type:	Unnotched			Machined Slit													
	Notch Size:	N/A	N/A	N/A	0.250	0.250	0.438	0.500	0.500	0.750	0.875	0.875	1.250	2.000	2.500	8.000	9.000	12.000
	Width:	1	2	3	1	2	3.5	2	3.5	3	3.5	3.5	10	8	10	36	36	60
	Length:	12	12	12	12	12	12	12	12	12	12	12	30	24	30	90	90	150
	W/2a:	N/A	N/A	N/A	4	8	8	4	7	4	4	4	8	4	4	4.5	4	5
	Test Temperature:	RT	RT	RT	RT	RT	RT	RT	RT	RT	RT	-75F	RT	RT	RT	RT	RT	RT
Material	Laminate																	
AS4/938 Tape	Crown3-Hoop			5						5				4				
AS4/938 Tow	2/4/6-Axial	3	3		3	3					3				2			
	2/4/6-Hoop	3	3		3	3					3				2			
	Crown3-Axial		4		3						2	2						
	Crown3-Hoop		4	5	3					5	2	1		5	2			1
	Crown4-Axial	3			3						3				2			1
25%-Glass Hybrid	Crown3-Axial		4		4						2	2						
	Crown3-Hoop		4		4						2	2			2			
	Crown4-Axial	3			3						3				2			1
Hoop Hybrid	4/4/4-Axial		3															
	4/4/4-Hoop		3		3			2	3		3				2			
IM7/8551-7 Tape	Crown3-Axial	3				3	3	2			3		2		2	1		
	Crown3-Hoop	3				3	3	2			3		2		2		1	

Layups:
Crown3 = [45/-45/90/0/60/-60/90/-60/60/0/90/-45/45]
Crown4 = [45/-45/90/0/60/-60/15/90/-15/-60/60/0/90/-45/45]
2/4/6 = [-45/90/45/90/0/90]s
4/4/4 = [-45/90/45/0/0/90]s (90-deg plies are 50% AS4/938 and 50% S2/938 with 8-tow repeat unit)
Note: 0-deg direction = Axial direction

Figure 2. Specimen configurations and number of replicates for tension fracture testing.

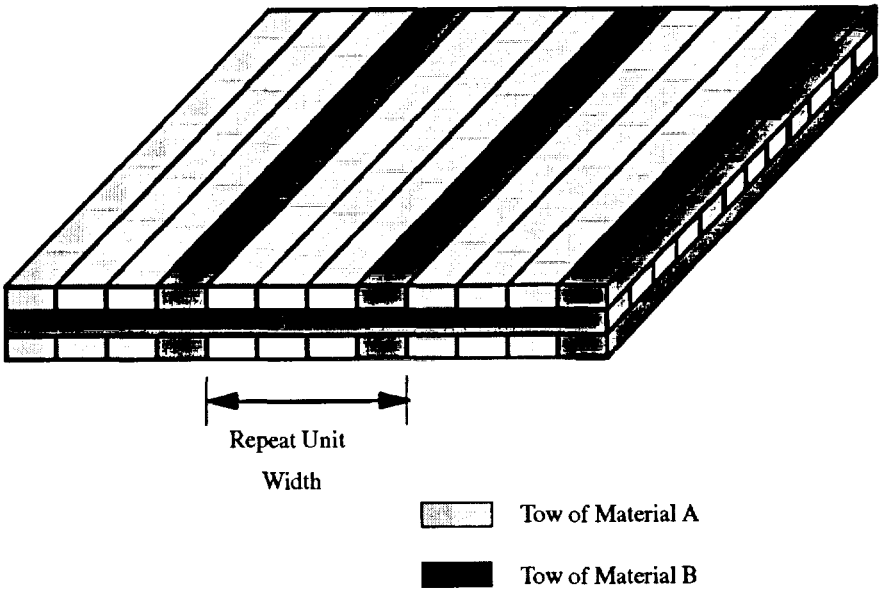

Figure 3. Schematic of intraply hybrid material.

Other variables considered included notch length, *W/2a*, test temperature, and load rate. Notch sizes ranged from 0.25 to 12.0 inches. Specimens with *W/2a* = 4 and 8 were tested to further evaluate the limits of isotropic finite width correction factors. Limited tests were conducted at reduced temperature (-75°F). The notch type for all tests was limited to machined central slits, for manufacturing convenience and repeatability, and since previous data provided some, although not conclusive, indications that machined slits were

either equivalent or conservative for some materials when compared with sharp penetration damage.

The two 5-stringer fracture panel configurations are illustrated in Figure 4. Both panels were identical in geometry and layup, with hat stringers at 14 inch spacing. The first panel was fabricated entirely from AS4/938 tow and the second using an intraply hybrid of 75% AS4/938 and 25% S2/938 with an 8 tow repeat unit. Both contained a centered, single-bay skin notch (14 in.) that also severed the central hat stringer.

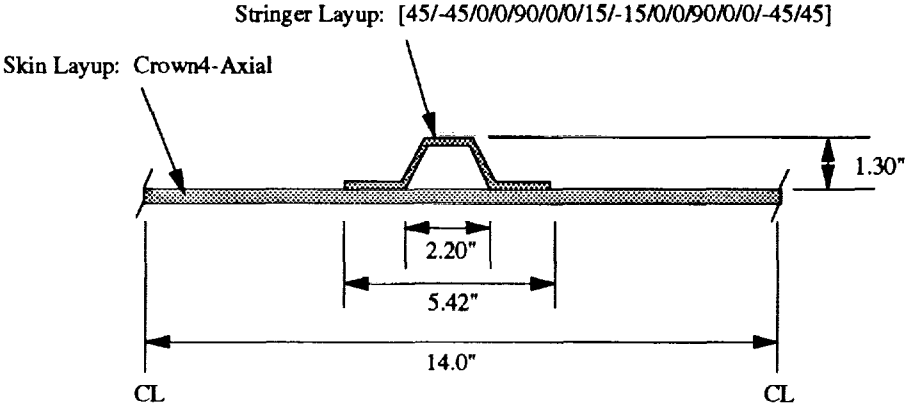

Figure 4. Stiffened fracture panel configurations.

All laminates in the test matrix were fabricated from material with a fiber volume of approximately 57% (corresponding to a resin content of 35% for graphite/epoxy systems). The fiber tows used in the tape materials were 12K. To maintain approximately equal tow spread for all intraply hybrid fiber types, tow-placed laminates were fabricated using 6K tows of AS4 and 20-end 750 yd./lb. S2-glass.

Panel Fabrication

The tow-placed laminates were fabricated on the Hercules 7-axis fiber placement machine using a 32-tow Cut-and-Add head. The tape panels were fabricated from 12 inch wide prepreg tape using standard hand layup techniques. All panels were autoclave cured at 350°F. The nominal cured ply thickness for both tow and tape materials was 0.0074 in. Through transmission ultrasonics was used to non-destructively inspect each panel after cure to ensure laminate quality. Measurements indicated that all panels fabricated were within specified limits.

The stiffened panels were also fabricated on the Hercules 7-axis fiber placement machine using the 32-tow Cut-and-Add head. The skin and stringer charges were tow-placed separately. The stringer charges were then trimmed and hot-drape-formed at approximately 150°F to the hat-section shape. The panels were assembled, with flexible aluminum-wafer and silicone rubber stringer mandrels (Ref. 6) being used for the non-hybrid and hybrid panels, respectively. Both panels were then covered with a thin graphite caul plate that included the intended stringer cross-section, bagged, and cured at 350°F.

Difficulties were encountered in removing the aluminum-wafer stringer mandrels from the non-hybrid panel, resulting in many areas of delamination along the skin/stringer bondline. In only one section of the test panel, however, did the delamination extend beyond the adhesive noodle, as shown in Figure 5. This region was remote from the crack-tip, and mechanical fasteners were placed through this approximately 12 in. long partial delamination to preclude premature failure of the test panel. The silicone mandrels were removed without incident from the hybrid panel, and no significant delaminations were noted.

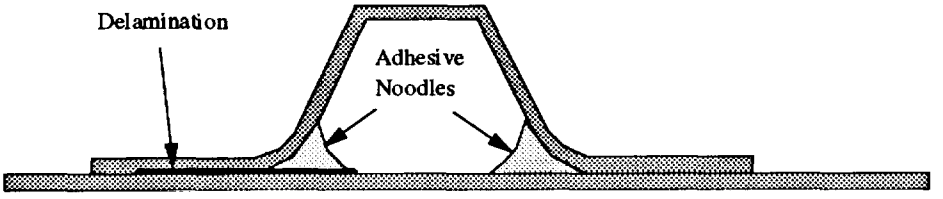

Figure 5. Location of skin/stringer disbond prior to panel testing.

Specimen Machining

The coupons were cut to slightly oversized dimensions using a band saw, then sanded to final dimensions. A 125 surface finish was designated for all cut edges. The slits were created by drilling two 0.070 inch diameter holes at the crack tip locations, then connecting them using an abrasive waterjet cutter.

The 10 in. x 30 in. coupons were tabbed with 10 in. x 3 in. tabs on both sides of each end to preclude failure in the grips. The tabs were fabricated from various graphite/epoxy materials with each tab having a nominal thickness of approximately 0.070 inches. They were bonded to the test specimens with a 0.010 inch thick 250°F cure film adhesive. Peel plies were used on the tab bonding surfaces, while the test specimens were prepared for bonding by lightly grit blasting the bonding surfaces, followed by a solvent wipe to remove any loose material.

The three 60 in. x 150 in. flat unstiffened panels were prepared in a manner similar to the 10 in. x 30 in. coupons. All three panels featured a center slit created by drilling two 0.070 inch diameter holes 12 inches apart, which were subsequently connected using an abrasive waterjet cutter. Precured 60 in. x 13.2 in. tabs fabricated from graphite/epoxy prepreg tape with a [-45/45/-45/45/0/90/0/45/-45/45/-45] stacking sequence were adhesively bonded on both sides of each end with a 0.010 inch thick 250°F cure film adhesive.

The two 60 in. x 150 in. flat stiffened panels were shortened to (a) eliminate delaminations caused by stiffener mandrel removal on the AS4/938 panel and (b) enable the panels to fit within the test frame constraints. The as-tested length of the AS4/938 panel was 126 in. while the hybrid panel was 137 in. long. As with the other panels, two 0.070 in. diameter holes were drilled 14 inches apart in the center of the panel to locate the crack tips. These holes were then joined using a hand-held narrow kerf diamond cutoff saw. As previously mentioned, the center stringer was severed resulting in the center slit extending to the

middle of each adjacent skin bay. Doublers 14.5 in. long fabricated from graphite/epoxy 250°F cure prepreg plain weave fabric with a $[\pm 45,0/90,\pm 45,0/90,\pm 45]_{10}$ stacking sequence were secondarily cured on the panel, with a 0.005 in. thick layer of 250°F cure film adhesive used between the doubler plies and the panels to improve the doubler bond. The doublers extended between stiffener flanges on the stiffened side only. This, combined with machined aluminum grip plates, resulted in load application to the panel neutral axis. Sixty 0.375 in. diameter fasteners were used to attach aluminum grip plates to each end of the panel. Load was directly introduced into the skin and stiffener flanges, but no attempt was made to directly load the stiffener webs or caps.

Test Procedures

The smaller coupons were loaded in monotonic tension to failure. Strain measurements were made using either remote extensometers or strain gages. The large unstiffened and stiffened panels tests were conducted as a series of load-unload sequences to successively higher loads. Non-destructive inspections, in the form of x-rays and/or pulse-echo, were performed after each unloading. These larger panels were extensively instrumented, including strain gages and shadow Moiré (to measure out-of-plane displacements of the crack edges).

UNSTIFFENED TEST RESULTS

The average nominal failure stress (i.e., failure load divided by the product of the number of plies and the nominal ply thickness) for each specimen and unstiffened panel configuration is listed in Figure 6. The following discussions will highlight the important findings.

Coupon Tests

A major finding during the second phase of the ATCAS tension fracture studies, observed at MIT by Lagace and McManus under ATCAS subcontract, was the confirmation of the previously observed 10-25% tension fracture improvements of tow-placed laminates over similar tape laminates, for a layup other than that tested in previous ATCAS experiments. These results are shown for a quasi-static strain rate in Figure 7. In addition to its higher fracture strength, the tow-placed laminate was found to exhibit less strength reduction with increasing strain rate than does its tape counterpart for strain rates up to 2.04 in./in./min. The importance of strengths at higher strain rates is related to the potential high-speed blade penetration event and the ensuing cabin-pressure release.

	Notch Type:	Unnotched			Machined Slit												
	Notch Size:	N/A	N/A	N/A	0.250	0.250	0.438	0.500	0.500	0.750	0.875	0.875	1.250	2.000	2.500	8.000	9.000	12.000
	Width:	1	2	3	1	2	3.5	2	3.5	3	3.5	3.5	10	8	10	36	36	60
	Length:	12	12	12	12	12	12	12	12	12	12	12	30	24	30	90	90	150
	W/2a:	N/A	N/A	N/A	4	8	8	4	7	4	4	4	8	4	4	4.5	4	5
	Test Temperature:	RT	RT	RT	RT	RT	RT	RT	RT	RT	RT	-75F	RT	RT	RT	RT	RT	RT
Material	Laminate																	
AS4/938 Tape	Crown3-Hoop			89.21						40.40				29.46				
AS4/938 Tow	2/4/6-Axial	58.02	59.09		39.41	41.29					30.35				25.00			
	2/4/6-Hoop	142.75	131.27		75.04	91.59					63.71				48.14			
	Crown3-Axial		58.03		35.03						30.03	27.86						
	Crown3-Hoop		83.67	85.47	65.45					50.88	51.98	51.68		42.06	38.90			22.51
	Crown4-Axial	66.02			40.13						33.29				29.91			21.98
25%-Glass Hybrid	Crown3-Axial		53.24		30.93						32.82	28.79						
	Crown3-Hoop		76.02		57.95						50.94	52.87			41.06			
	Crown4-Axial	60.08			39.26						35.35				31.80			27.10
Hoop Hybrid	4/4/4-Axial		94.91															
	4/4/4-Hoop		80.87		51.16			50.03	58.34		46.87				40.03			
IM7/8551-7 Tape	Crown3-Axial	81.84				51.06	50.30	44.18			39.13		40.12		31.96	22.49		
	Crown3-Hoop	130.14				83.47	72.01	62.73			55.18		49.84		37.10		18.57	

Layups:
Crown3 = [45/-45/90/0/60/-60/90/-60/60/0/90/-45/45]
Crown4 = [45/-45/90/0/60/-60/15/90/-15/-60/60/0/90/-45/45]
2/4/6 = [-45/90/45/90/0/90]s
4/4/4 = [-45/90/45/0/0/90]s (90-deg plies are 50% AS4/938 and 50% S2/938 with 8-tow repeat unit)
Note: 0-deg direction = Axial direction

Figure 6. Nominal failure stresses for unstiffened fracture tests.

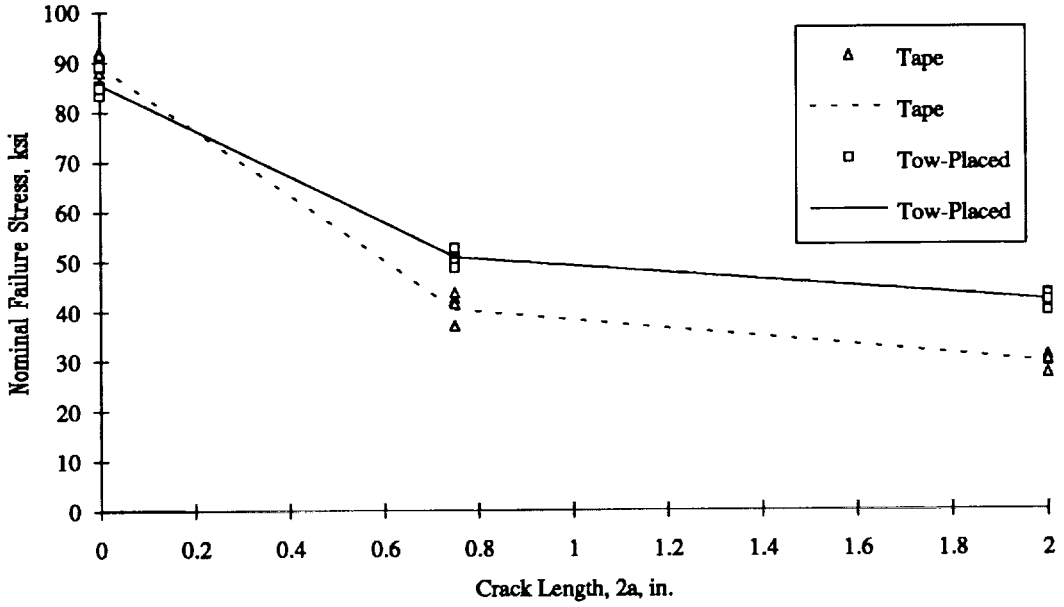

Figure 7. Fracture strengths of tow-placed and tape AS4/938 laminates measured under MIT subcontract (Lagace and McManus).

Two intraply hybrid concepts were considered at the coupon level. In the first concept (i.e., 25%-Glass Hybrid), all plies were hybridized with 25% S2-glass. In the second (i.e.,

Hoop Hybrid), only the hoop direction plies were hybridized (50% S2-glass), similar to buffer-strip concepts widely studied in the past (e.g., Refs. 7, 8). All tests of the Hoop Hybrid were conducted with the notch perpendicular to the glass strips. As shown in Figure 8, the 25%-Glass Hybrid had superior fracture performance for the notch sizes below 2.5 inches, but its advantages over the Hoop Hybrid diminish with increasing crack length. At notch lengths above 2.5 inches, the Hoop Hybrid is likely to have the higher strengths. A significant drawback to this material concept, however, is the directionality of its improved fracture performance; notches oriented other than perpendicular to the glass strips will likely result in significantly lower strengths. Damage progression was shown by x-rays to be significantly different for the two hybridizing concepts. Growth in the Hoop Hybrid was severely antisymmetric, appearing to follow the glass strips, while growth in the 25%-Glass Hybrid was more uniform around the crack tip.

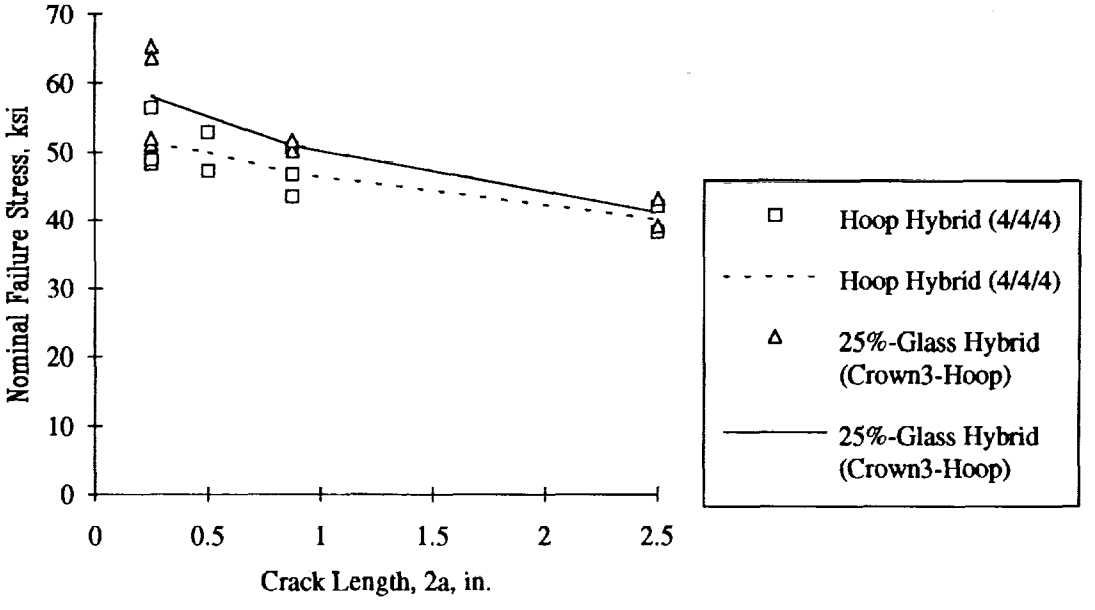

Figure 8. Failure strengths of intraply hybrid concepts.

Results obtained comparing notched strengths at reduced and ambient temperatures are shown in Figure 9. For the AS4/938 material, the more 0°-dominated laminate (Crown3-Hoop) exhibited no reduction in strength due to the reduced temperature, while the 90°-dominated laminate (Crown3-Axial) exhibited a 7% decrease. This likely relates to a combination of (a) the reliance of the 90°-dominated laminate on the matrix for load transfer around the notch and (b) the embrittlement of the matrix at the reduced temperature. Similar results were observed for the 25%-Glass Hybrid material.

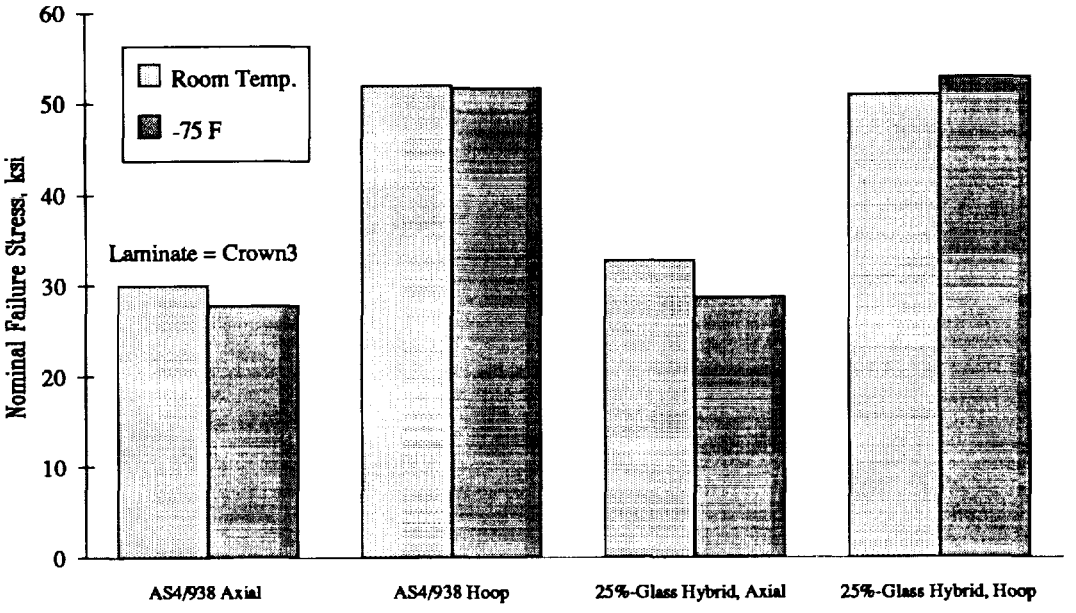

Figure 9. Effect of temperature on tension fracture strength.

Large Panel Tests

Five laminate/material combinations were tested with notch sizes of 8 inches or greater. Small-notch coupons were also tested for each of these combinations, and the results are summarized in Figure 10. Each point in the figure represents the average value of all tests conducted with $W/2a$ between 4.0 and 5.0 for a specific notch size and laminate/material combination. A considerable range of behavior was observed, and confirms earlier ATCAS findings that the small-notch strength of a particular laminate/material combination had little direct relationship with its large-notch strength. Other relationships observed in the data are discussed in the following paragraphs.

The effect of varying the material for each of two laminates is shown in Figures 11 and 12. In Figure 11 it can be seen that, for the Crown3-Hoop laminate, the IM7/8551-7 material provided higher small-notch strengths than the AS4/938 but lower strengths at notch lengths above approximately 2 inches. This confirms earlier ATCAS findings of a cross-over. It is also similar to the trade-off between yield strength and fracture toughness observed in aluminum alloys, where the small notch strengths and large notch strengths of the composites assume the roles of the yield strength and fracture toughness of the aluminum, respectively. A similar compromise is seen between the AS4/938 and the 25%-Glass Hybrid for the Crown4-Axial laminate in Figure 12, where the former has higher strengths with notch lengths below approximately 0.5 inches, and lower strengths above. The 25%-Glass Hybrid was nearly notch-insensitive, exhibiting only a 20% reduction in strength as notch lengths varied from 0.25 to 12 inches.

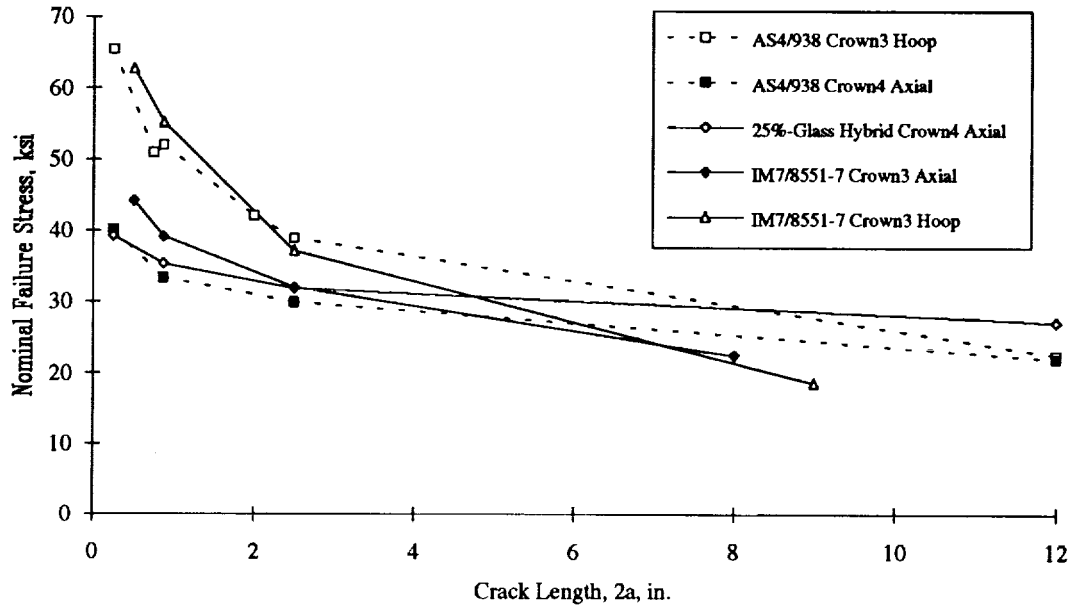

Figure 10. Tension fracture performance of laminate/material combinations tested with large notches.

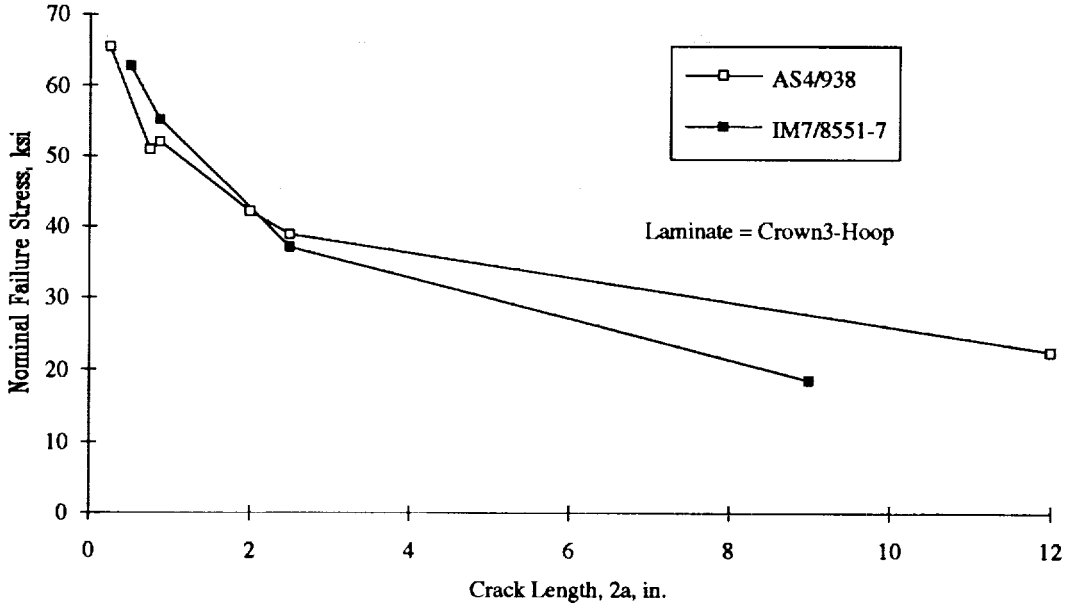

Figure 11. Material influence on fracture strength for the Crown3-Hoop laminate.

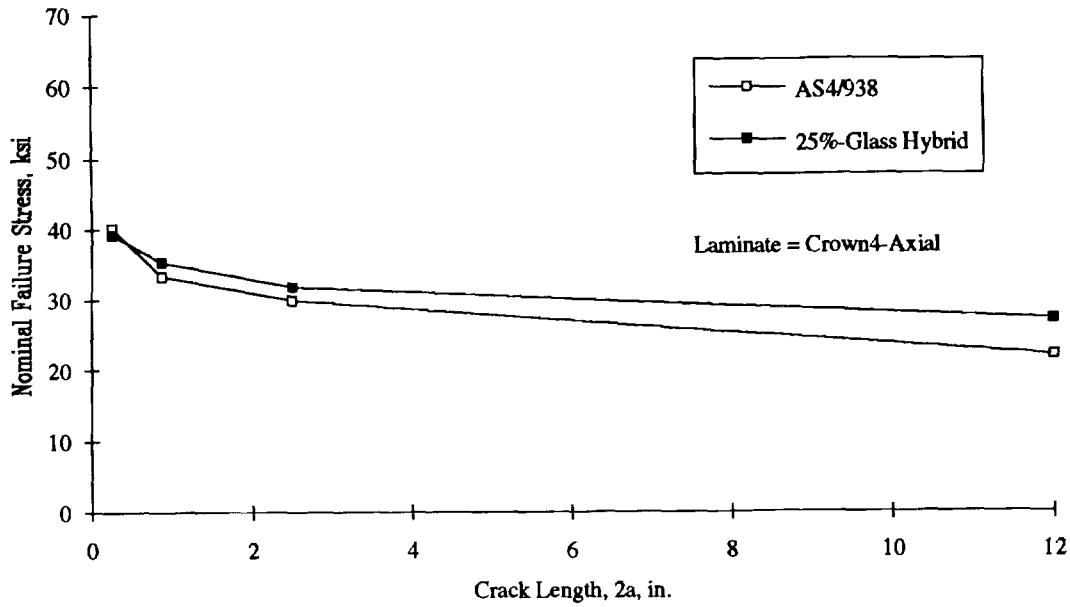

Figure 12. Material influence on fracture strength of the Crown4-Axial laminate.

The effect of varying the layup for each of two materials can be seen in Figures 13 and 14. A similar trade-off between small-notch and large-notch strengths is observed for both the AS4/938 and IM7/8551-7 material systems. In both cases, the laminate with the higher modulus parallel to the loading direction exhibited strengths that were larger for small notches but lower for large notches. The notch size at which the cross-over occurs, however, is significantly larger than that observed for material differences. The stress versus strain plots for notched panels with differing layups show that relatively soft laminates have significantly higher failure strains and work to fracture. This observation is an important finding in support of composite skin design. Additional discussions on the use of soft-skin/hard-stiffener designs to achieve structural damage tolerance is given in Reference 1.

The results of these laminate/material combinations were also compared by observing the convergence of the classical stress intensity factor (K_{IC}) with increasing crack length, as shown in Figure 15. As was observed in previous ATCAS studies, K_{IC} increased with notch length for all laminate/material combinations. In the extreme cases, the stress intensity factor of the stiffer of the two IM7/8551-7 laminates had converged to an approximately constant value at a notch length of approximately 2 inches while that of the 25%-glass hybrid was still increasing rapidly at a 12 inch notch length. A similar requirement for large notch testing has been observed in obtaining converged plane-stress fracture toughnesses for ductile aluminum alloys, as illustrated in Figure 16.

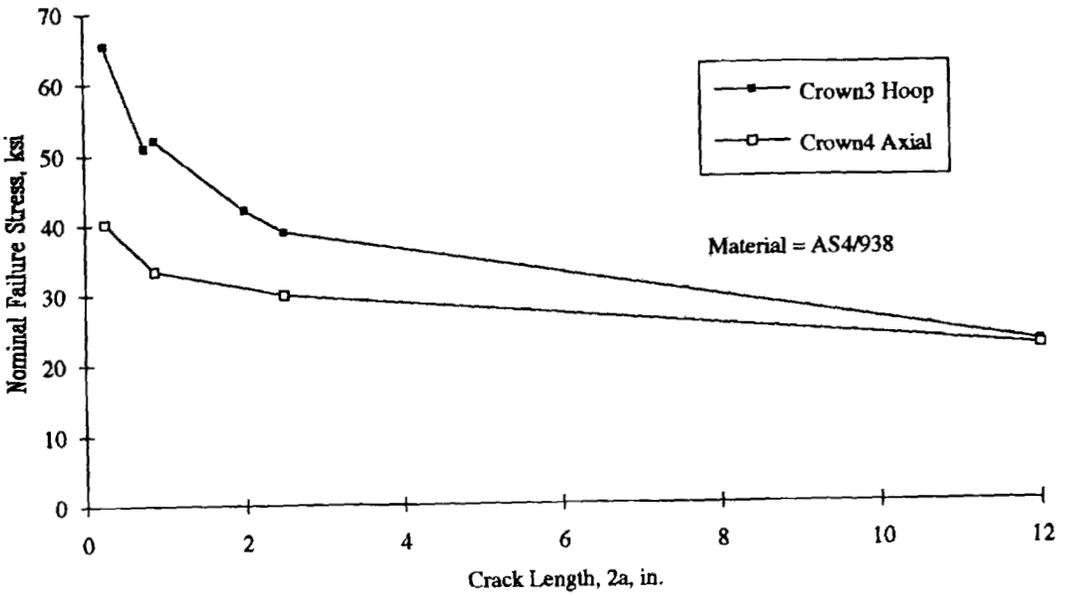

Figure 13. Laminate influence on fracture strength of AS4/938.

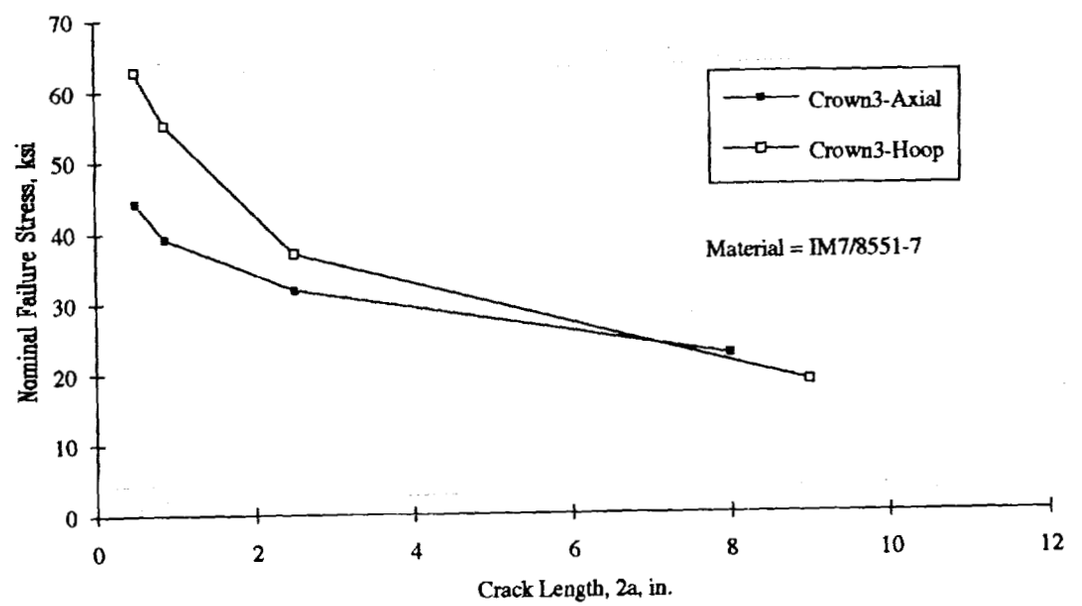

Figure 14. Laminate influence on fracture strength of IM7/8551-7.

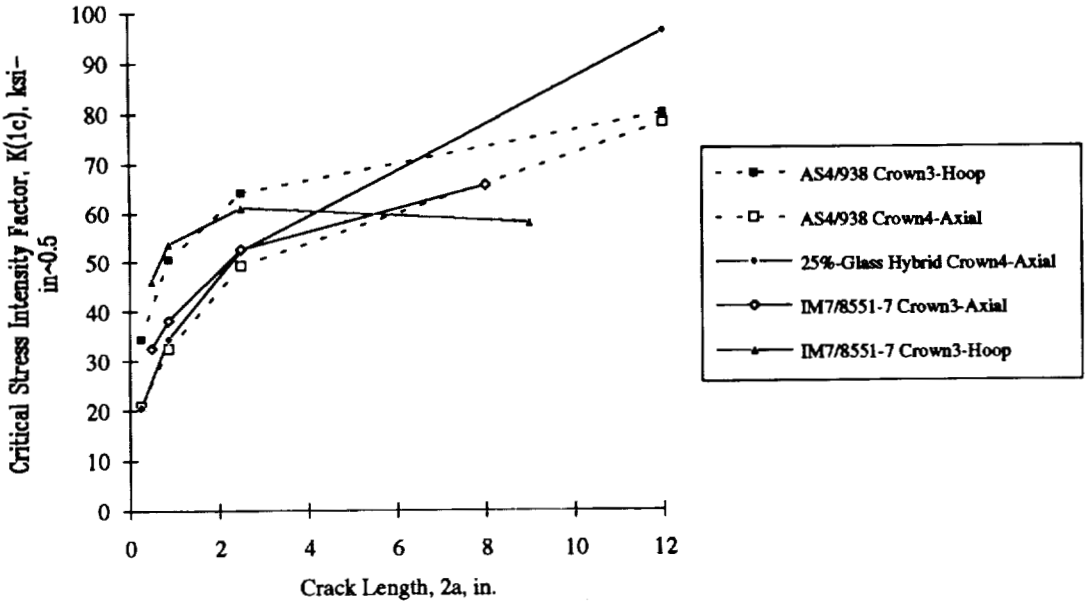

Figure 15. Convergence of classical fracture toughness with increasing crack length.

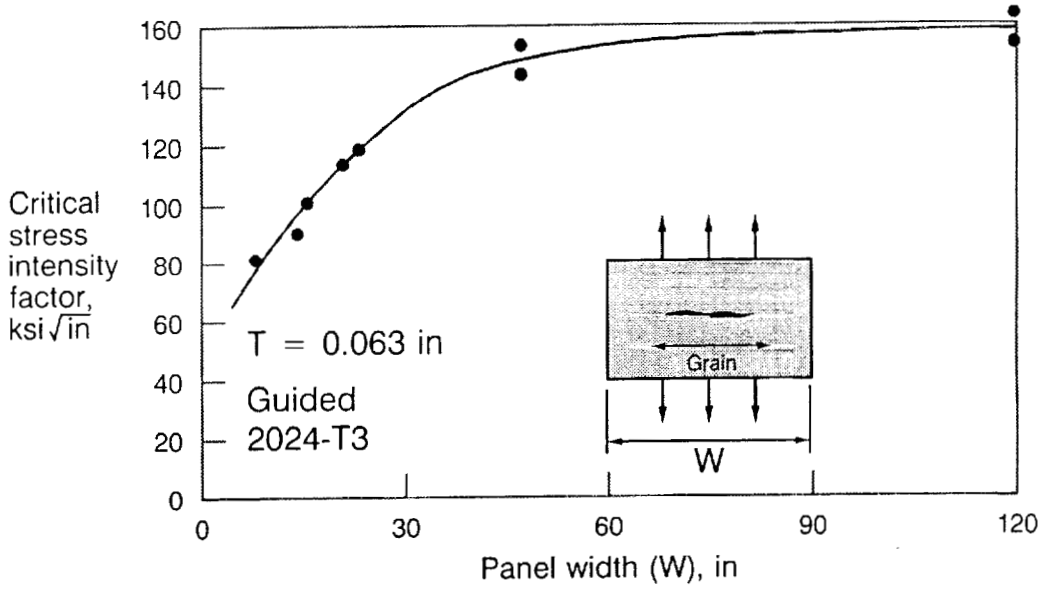

Figure 16. Plane-stress fracture toughness convergence of 2024-T3 (Ref. 9).

ANALYSIS OF UNSTIFFENED RESULTS

Finite Width Corrections

Correcting failure strengths for finite width effects provides the basis for comparison of different specimen configurations. Numerical methods have been employed to show that isotropic finite width correction factors (FWCF) differ from their orthotropic counterparts by less that 3% for specimen-width-to-crack-length ratios (*W/2a*) greater than 2 (Refs. 10, 11). Any of the several expressions for isotropic FWCFs may therefore be used. In the current studies, the nominal notched strengths for specimens with *W/2a* = 4 and 8, corrected for finite width according to

$$\sigma_N^{\infty} = FWCF * \sigma_N \tag{1}$$

where

$$FWCF = \sqrt{\sec\left(\frac{\pi a}{W}\right)} \tag{2}$$

(Ref. 10) were used to further assess the validity of using isotropic FWCFs. The isotropic FWCFs for these two cases are approximately 4% and 1%, respectively. If the finite-width correction factor properly accounts for all differences between the two specimen geometries, the datasets for each of these *W/2a* values should fall on a single curve when the corrected strengths are plotted versus notch length.

Four laminate/material combinations were evaluated in such a manner. For each of these combinations, the FWCFs were underpredicted for the W/2a = 4 specimens, although by less than previously observed for *W/2a* = 2 data when compared with *W/2a* = 4. Representative comparisons are contained in Figures 17 and 18. As indicated in Reference 3, specimen edge-delamination, crack-tip softening due to matrix damage, and buckling adjacent to the unsupported crack surfaces may result in larger interactions between the notch-tip stress field and the specimen edges than analytically predicted.

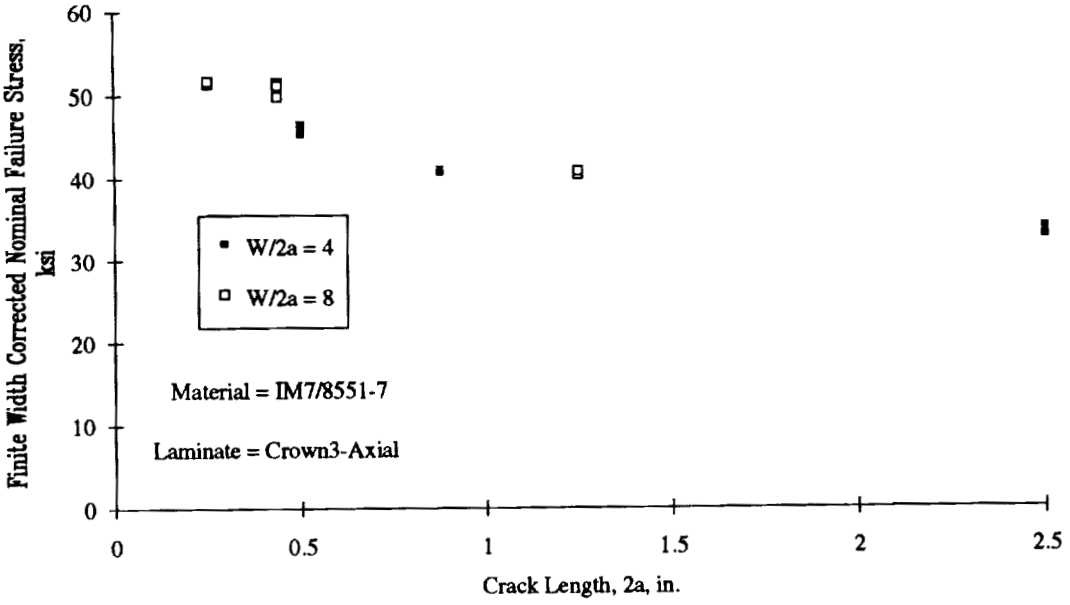

Figure 17. Comparison of finite width corrected strengths for IM7/8551-7 specimens with *W/2a* = 4 and *W/2a* = 8.

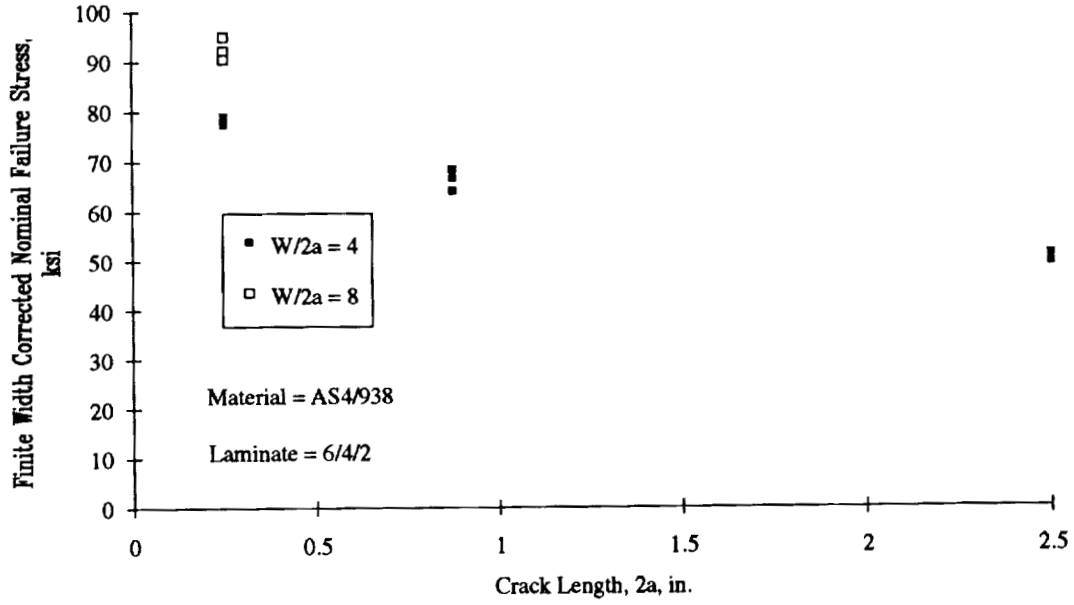

Figure 18. Comparison of finite width corrected strengths for AS4/938 specimens with *W/2a* = 4 and *W/2a* = 8.

Comparison with Experimental Strengths

Previous evaluation of strength prediction models focused on four primary candidates: linear elastic fracture mechanics (LEFM), Whitney-Nuismer point stress (WN), Poe-Sova (PS), and Mar-Lin (ML). Reference 3 contains a brief discussion of these methods and compares the functionality of each. Several major behavioral characteristics were noted when all methods were calibrated through a single notch-length/failure-strength point. For this calibration, the unnotched strength used in the LEFM, WN and PS methods was assumed to be the product of the laminate modulus and the fiber failure strain. For the ML method, the exponent was assumed, leaving only the composite fracture toughness to be determined.

The WN and PS methods were found to be functionally equivalent. The effect of the characteristic dimensions used in these methods is to reduce the small notch strength predictions from the parent LEFM curve. As crack lengths increase, differences between these characteristic-dimension methods and LEFM converge to a constant value that is small in comparison with the prediction. The order of the stress singularity in the vicinity of the crack tip controls the large notch strength, with reduced singularities predicting higher strengths. Comparison with experimental results indicated that these reduced singularities were required to accurately predict the large notch strengths from smaller notch strengths for most material/laminate combinations tested. The lone exception to this finding was an IM7/8551-7 laminate.

Similar evaluations were conducted in the current study for the 5 laminate/material combinations for which large notch strengths were obtained. In each case, the LEFM, PS, and ML methods were calibrated through the average strength with a 2.5 in. notch. The ML exponent, n, was varied to determine the singularity providing the best prediction of the largest-notch strength. The results for the two IM7/8551-7 laminates are shown in Figures 19 and 20. For the stiffer Crown3-Hoop laminate, LEFM and PS ($n = 0.5$ for both methods) provided the best correlation with the largest notch strengths, while for the less-stiff Crown3-Axial laminate, the ML method with $n = 0.3$ provided good results. A similar *trend* was observed in the results obtained from the AS4/938 laminates, shown in Figures 21 and 22, although at a reduced singularity value. The stiffer Crown3-Hoop laminate required $n = 0.3$, while the softer Crown4-Axial laminate required $n = 0.2$. The results for the hybrid laminate, shown in Figure 23, indicated the need for $n = 0.1$.

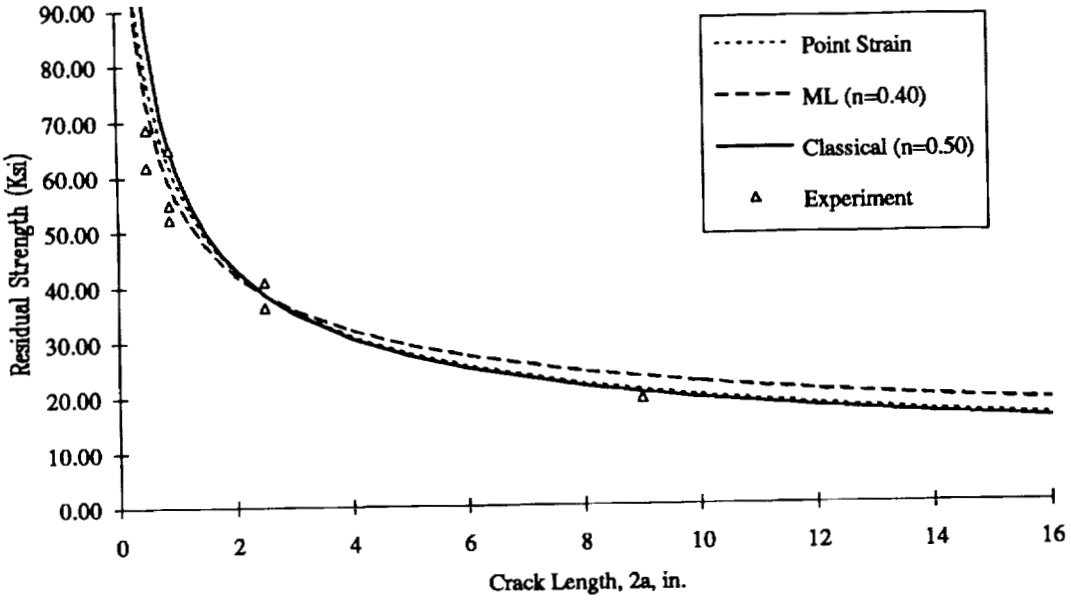

Figure 19. Comparison of IM7/8551-7, Crown3-Hoop experimental results with different failure criteria.

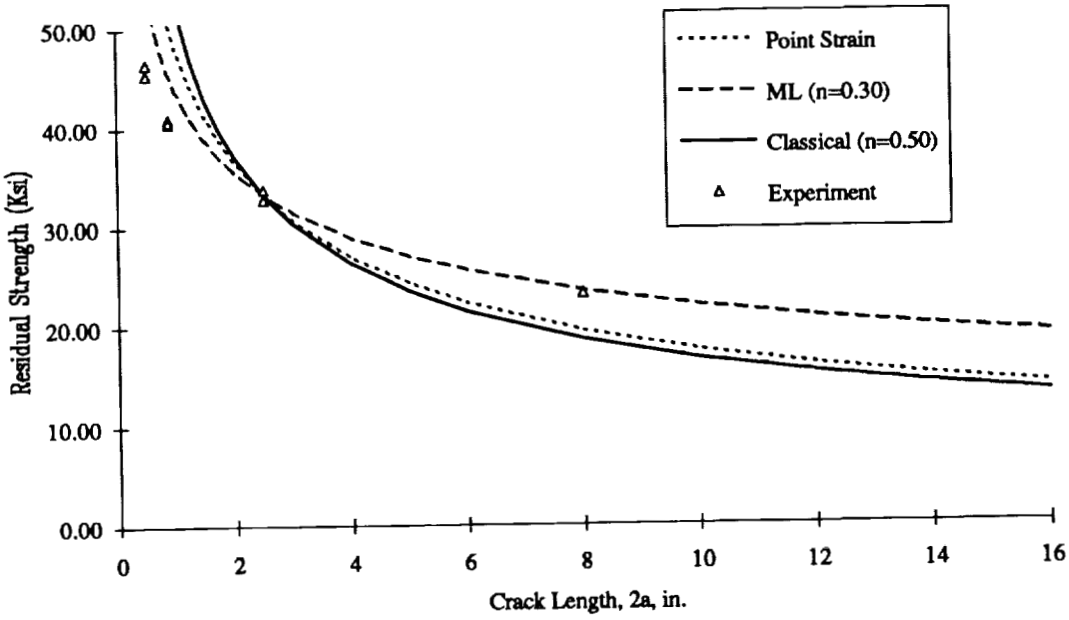

Figure 20. Comparison of IM7/8551-7, Crown3-Axial experimental results with different failure criteria.

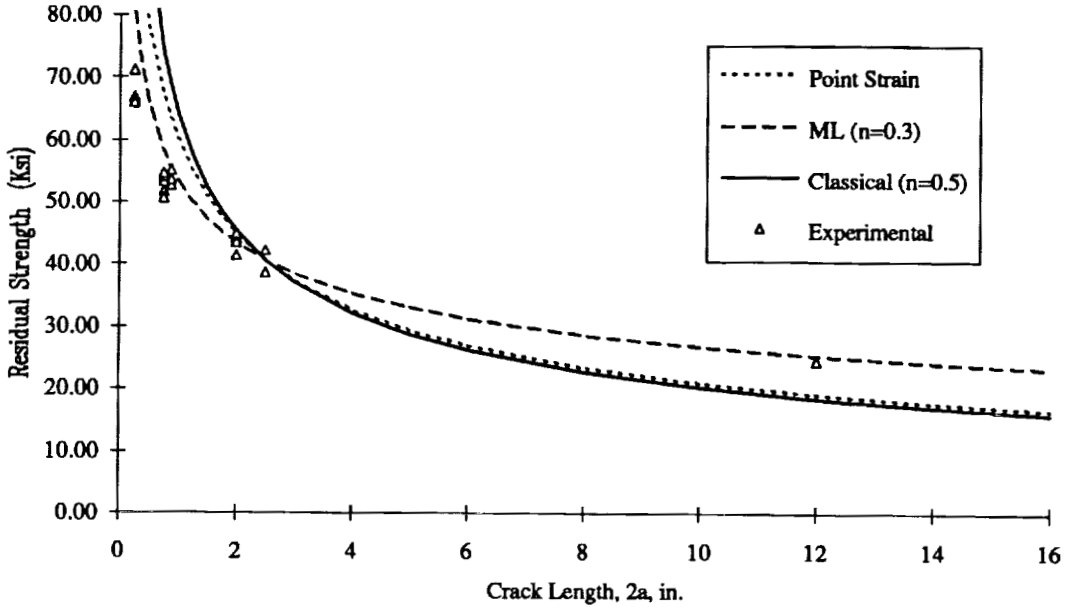

Figure 21. Comparison of AS4/938, Crown3-Hoop experimental results with different failure criteria.

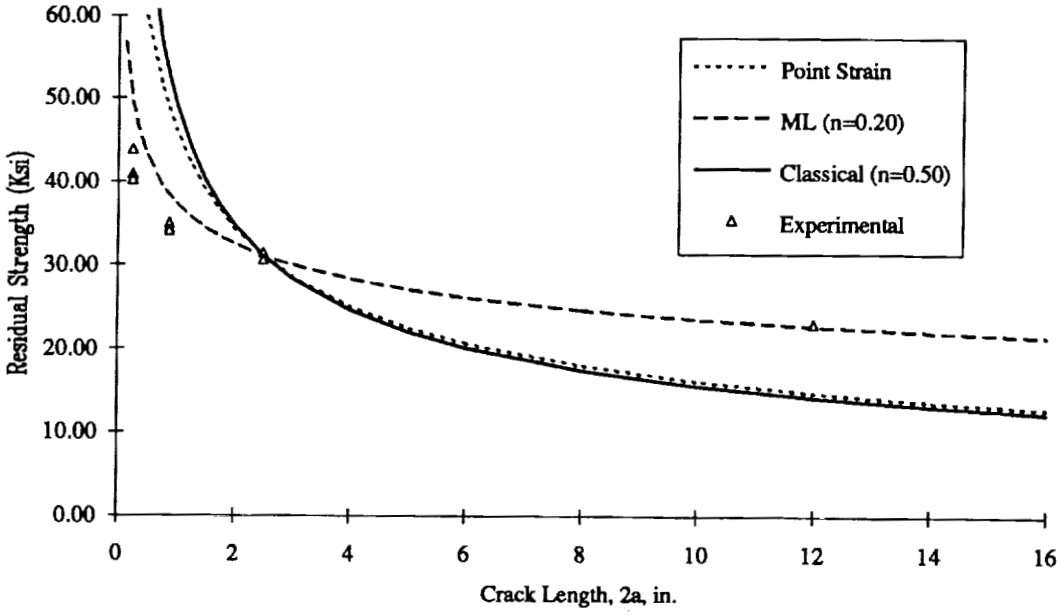

Figure 22. Comparison of AS4/938, Crown4-Axial experimental results with different failure criteria.

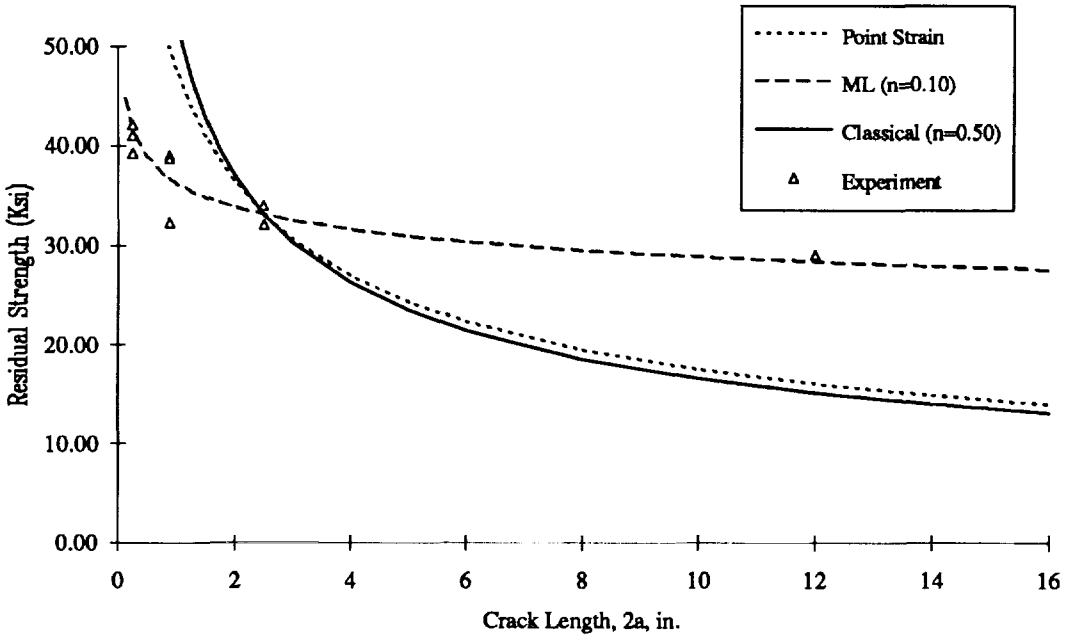

Figure 23. Comparison of 25%-Glass Hybrid, Crown4-Axial experimental results with different failure criteria.

The best-fit curves for the large-notch laminate/material combinations are shown in Figure 24. Variations in laminate and material can result in strengths that differ by a factor of 2 at large notch sizes representative of damage tolerance scenarios. For a stiffened panel design controlled by tension loads and large damage tolerance, selection of the most desirable laminate/material combination for skin and stiffener can help optimize weight and associated cost.

Most of these results suggest that methods based on the classical square-root stress-field singularity are not capable of predicting strengths for a large range of notch sizes, and that reduced-singularity methods may be more accurate. It is important to understand, however, whether the reduced-singularity stress fields are physically occurring, or whether the methods are just accounting for the effects of pre-failure damage. As discussed in reference to Figures 15 and 16, convergence to a true plane-stress fracture toughness (assuming a square-root singularity) may required very wide specimens. Net section yielding for narrow coupons or small notches tends to mask the true fracture properties of high toughness aluminum alloys such as 2024-T3 unless nonlinear methods (e.g., J-integral) are used to interpret test results.

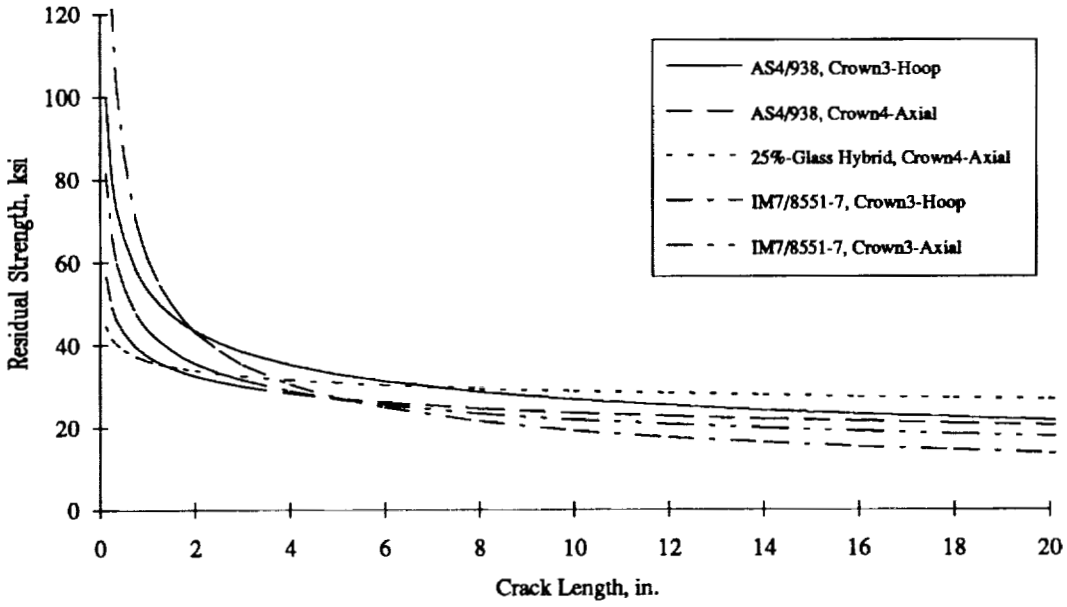

Figure 24. Comparison of theoretical predictions for all laminate/material combinations tested with large notches.

Comparisons with Measured Crack-Tip Strain Distributions

To determine the behavior of the crack-tip strain field, strains measured on the larger panels *prior to any crack-tip damage creation* were compared with theoretical prediction based on a relationships for a through-thickness crack in an specially orthotropic material subjected to mode I loading (Ref. 12). The strain predictions as a function of the distance ahead of the crack tip, r, are given by

$$\varepsilon_y(r) = \varepsilon_y^{\infty}\xi\sqrt{\frac{a}{2r}} * FWCF \tag{3}$$

where

$$\xi = \left[1 - \upsilon_{yx}\sqrt{\frac{E_x}{E_y}}\right], \tag{4}$$

FWCF is the finite-width correction factor given in equation (2), ε_y^{∞} is the far-field strain (taken as the measured value for predictive purposes), and a is the half-crack length. This relationship is accurate for distances ahead of the crack tip that are less than 10% of the crack length. A method for predicting *strain* distributions ahead of the crack tip in a reduced-singularity stress field was sought but not located in the literature.

The comparisons for each of the five large-notch laminate/material combinations are contained in Figures 25 through 29. As shown in Figure 25, the Crown3-Hoop IM7/8551-7 laminate most closely matches the predicted strain distribution. As previously discussed, failure predictions for this laminate/material combination were also most accurately predicted using the classical square-root stress-field singularity. All other laminates exhibited measured strains significantly higher than predicted over most of the distances considered. In several cases, the measured strains indicated a possible cross-over approaching the crack-tip, with the actual strains being lower than predicted. The higher-than-predicted strains may account for the previously discussed underprediction of finite width effects.

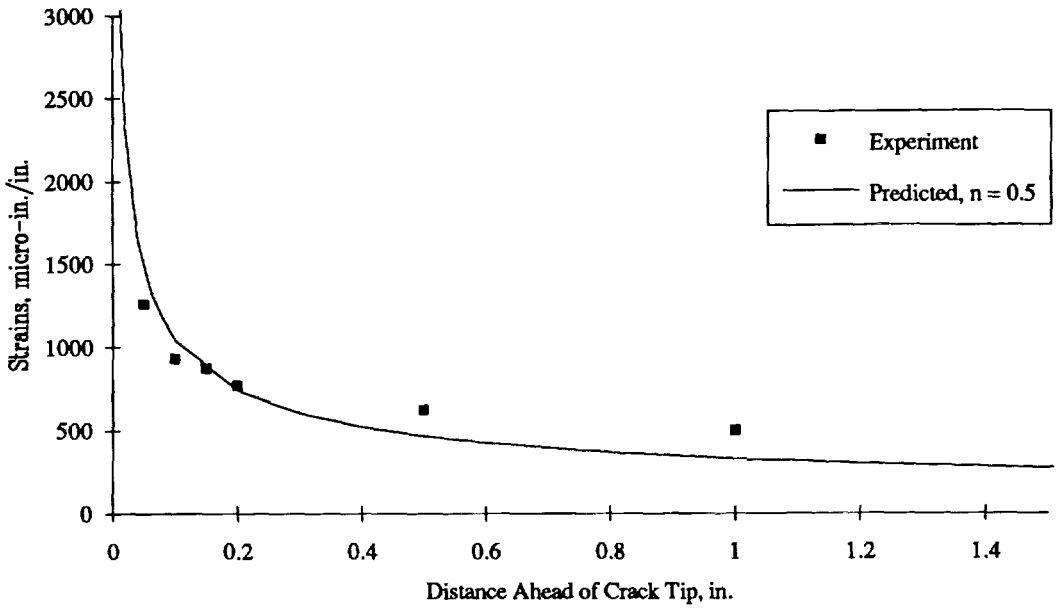

Figure 25. Comparison of predicted and measure crack-tip strains for IM7/8551-7, Crown3-Hoop laminate with an 9 inch notch.

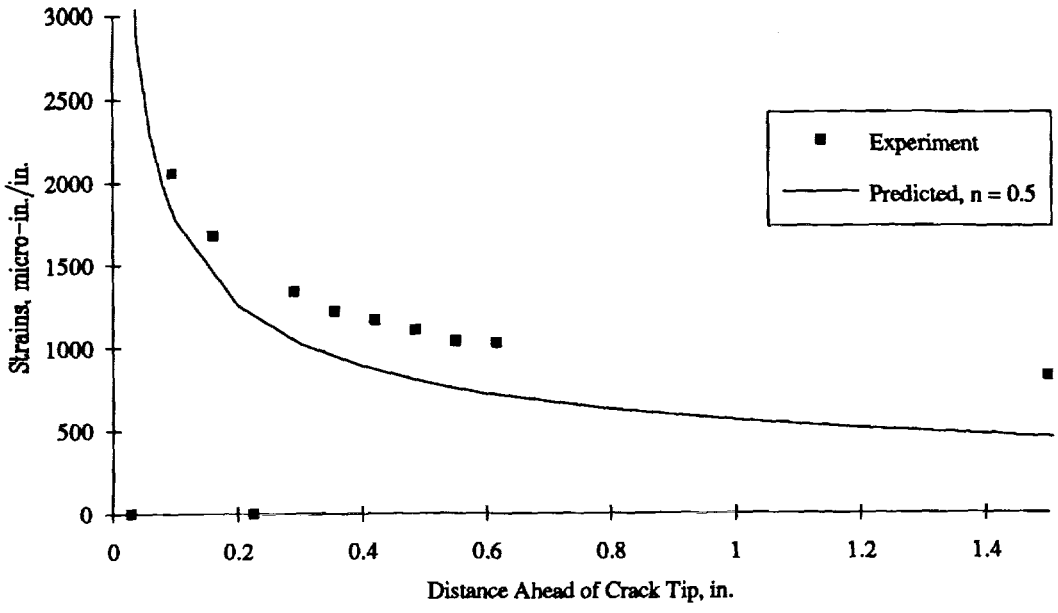

Figure 26. Comparison of predicted and measure crack-tip strains for IM7/8551-7, Crown3-Axial laminate with an 8 inch notch.

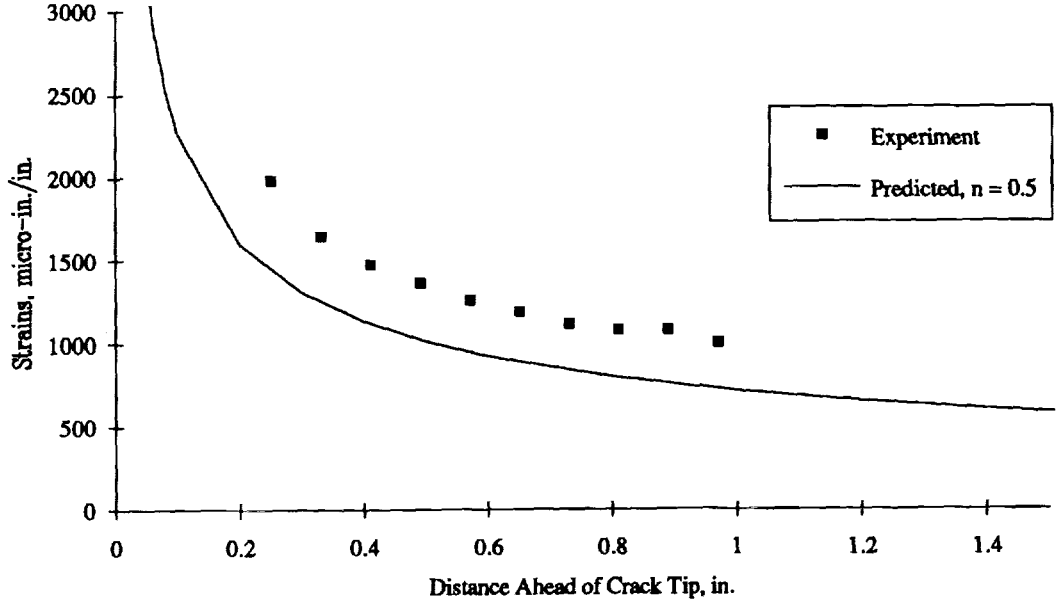

Figure 27. Comparison of predicted and measure crack-tip strains for AS4/938, Crown3-Hoop laminate with a 12 inch notch.

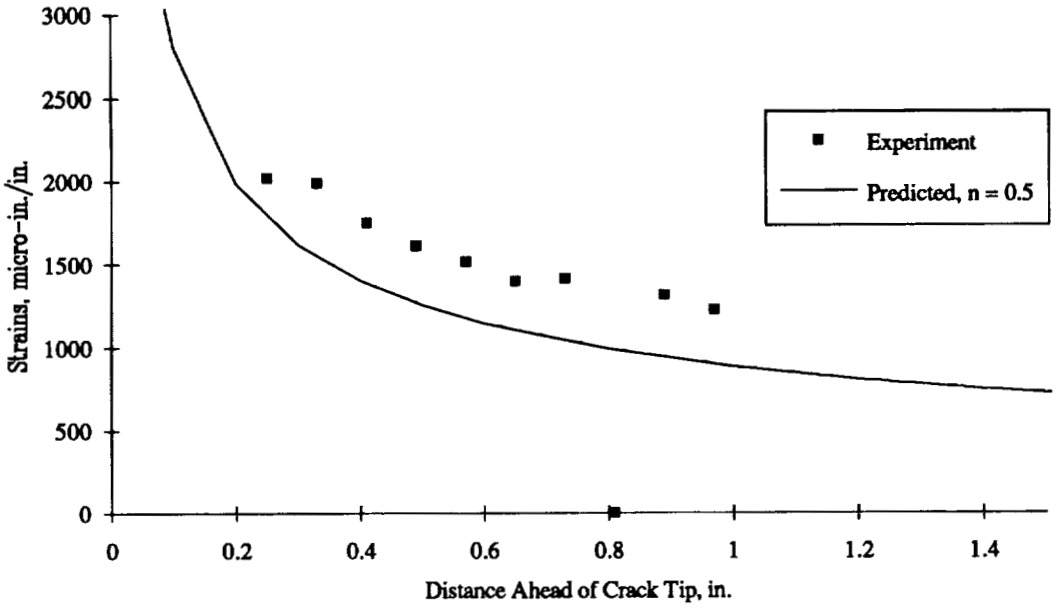

Figure 28. Comparison of predicted and measure crack-tip strains for AS4/938, Crown4-Axial laminate with a 12 inch notch.

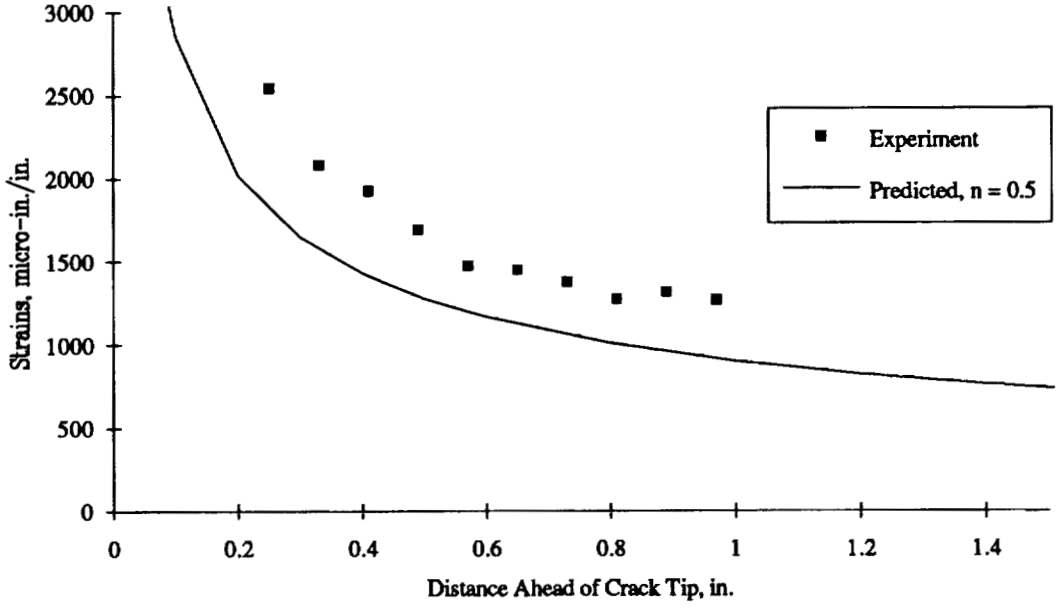

Figure 29. Comparison of predicted and measure crack-tip strains for 25%-Glass Hybrid, Crown4-Axial laminate with a 12 inch notch.

Another interesting characteristic, seen most clearly in Figures 28 and 29, are the undulations in the measure strains. Undulations of similar magnitude have been analytically observed over similar distances using simplified models of the larger scale of repeatable material inhomogeneity (Ref. 13). This implies that such inhomogeneities are affecting the response of the tow-placed laminates, and may be the cause of the high measured strains. In addition, it gives further support to the hypothesis that such inhomogeneities are related to the improved tension-fracture performance of the tow-placed laminates. Additional work is planned to generate more detailed models of tow-placed microstructure.

Alternative methods of accounting for the inhomogeneous microstructures of composites include generalized continua. Additional degrees-of-freedom that account for local rotation exist in Cosserat theories. These theories have found some application to mechanics problems involving stress concentrations in composites (e.g., Refs. 14, 15) and metals (Ref. 16). Attempts will be made to apply Cosserat theories to predict strain distributions shown in Figures 25 through 29.

Strain plots in this section suggest that past empirical modifications to fracture mechanics for thin composite laminates (e.g., characteristic dimension corrections, reduced singularities) correct for more than pre-catastrophic damage. Hypothetically, some composites smear the notch stress concentration over a wider area, resulting in stronger interactions with plate boundaries. As pre-catastrophic damage accumulates, such interactions are expected to become stronger. Future analysis developments are needed to quantify these effects, since they have important implications to scaling test results, material selection, and design for structural load sharing. Without analysis, expensive large-scale tests will be needed to show the full potential of composites.

STIFFENED PANEL RESULTS

Experimental

The failure strengths for the two 5-stringer flat fracture panels are compared with those for the unstiffened panels of the same skin laminate in Figure 30. Both panels failed in a nearly identical pattern. From each crack tip, a damage zone progressed in a stable manner within the skin to the adjacent stringer. Strain gages on adjacent stringers showed higher strains as skin damage approached, indicating increased load sharing that helped arrest the damage. The final failure sequence was initiated by the extension of a shallow skin delamination beyond the adjacent stringers, decoupling them from the majority of the skin, reducing load transfer to the stringers, and allowing catastrophic skin damage growth. Since the failure was controlled by the skin fracture (i.e., growth to the adjacent stiffeners and beyond, following loss of local load sharing with the stiffeners), it is not surprising that the 23% improvement observed between the graphite and hybrid panels in the unstiffened configuration was almost identically translated into the stiffened configurations.

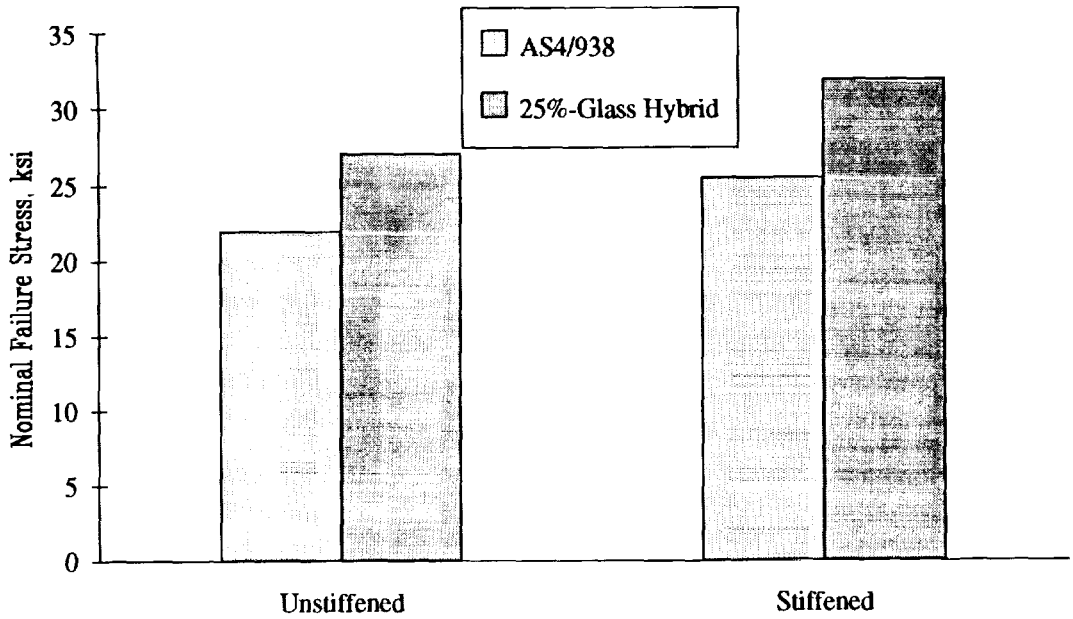

Figure 30. Failure strengths of unstiffened and stiffened fracture panels.

Analytical Considerations

A thorough discussion of failure predictions for the stiffened panels will be addressed in future documents. Briefly, however, accurate predictions for both of these panels were obtained using the following approach. The panel failure *strain* was obtained by predicting the fracture stress for a 2-bay (28 inch) notch in an *unstiffened* skin using the ML method and dividing this stress by the skin modulus. The ML parameters were obtained from small and large notch test results for the skin laminate. The panel failure *load* was then obtained by multiplying the predicted failure strain by the axial stiffness of the *stiffened* panel. This technique implicitly assumes (a) structural redundancy is such that with a severed element, the skin damage effectively grows to the adjacent stringers in a stable manner, and (b) after damage grows under the stiffener, load sharing becomes negligible and final failure occurs at the skin failure strain for a 2-bay notch.

While this method accurately predicted the two panels tested, more general methods are required to address the wide variety of structural arrangements and damage locations encountered on commercial fuselage. These methods must successfully address the three primary failure mechanisms: skin fracture, stiffener strength, and skin/stiffener debonding. The importance of skin fracture is indicated by its control of the failure of both stiffened panels. The effect of stiffening elements on load redistribution is also important, both in terms of (a) predicting stiffener strength and (b) the effects of skin stress reduction on damage progression. The significance of this latter issue is illustrated by the similarity of the damage-progression and failure sequences exhibited by the two stiffened-panel tests.

The ML method with variable singularity has demonstrated the ability to semi-empirically predict skin failure for a wider range of crack lengths. However, it is limited to use as an interpolation tool or as applied in Reference 3 for conservative extrapolation. In addition, if it does not accurately predict the stress and strain distributions prior to any crack-tip damage formation, it is not useful in predicting structural load redistribution as the damage zone progresses.

The finite element method appears to provide the flexibility and accuracy for a multitude of configurations encountered in aircraft structure. Two methods exist to account for the effects of damage progression on load redistribution in finite element models. Progressive damage methods that degrade various stiffness properties of individual elements as specified failure criteria are met (e.g. Ref. 17) have shown some success in modeling damage growth in specimen configurations. The magnitude of the calculations, however, provides a significant obstacle to incorporating them into the complex models required for stiffened structure.

Strain-softening models (e.g., Ref. 18, 19), however, appear to have the required simplicity. Such models have been successfully used in the reinforced concrete industry, and provide the ability to capture the global load redistribution that occurs as the crack-tip region is softened by damage formation, without the computational concerns of detailed progressive damage models. These strain softening models use a nonlinear stress-strain law that allows for a decreasing load-carrying capability of the material as strains increase beyond a critical value, as shown in Figure 31. A range of softening laws have been proposed. In finite element models, nonlinear springs can be used to simulate this behavior. The models can be calibrated using small-notch test results, then extended to large-notch configurations. Issues associated with modeling and calibrating bending stiffness reductions are being evaluated. These reductions are of concern for most structural configurations, where out-of-plane loading, load eccentricities, and bending loads are common.

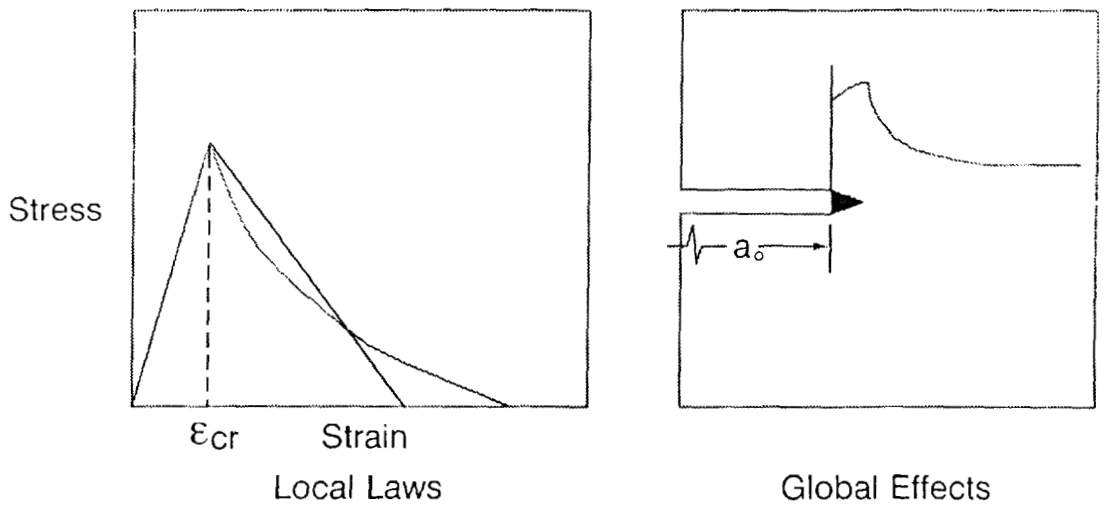

Figure 31. Strain-softening modeling approach.

CONCLUSIONS

Collaborative efforts between Boeing and NASA have continued to address the issues associated with transport fuselage pressure damage tolerance. Previous test results from 430 flat fracture coupons were augmented with an additional 200 coupons and extended into the large-notch and structural regimes with 5 large unstiffened panels and 2 large stiffened panels.

The additional tests confirmed some earlier findings and identified additional behaviors. Tow-placed laminates continue to exhibit 10 to 25% performance improvements over identical tape laminates. Large notch results indicated a trade-off between strength (small-notch strength) and toughness (large-notch strength), as shown in Figure 32. Higher strength but lower toughness resulted from toughened-resin materials and hard (0°-dominated) laminates. Lower strength and higher toughness was caused by brittle-resin materials, soft laminates and intraply hybridization with S2-Glass. Larger scales of repeatable material inhomogeneity appeared to result in improved toughness with little effect on strength. Matrix toughness appeared to have a larger influence on the behavior than laminate type.

Other performance characteristics were also identified. Temperature had little effect on 0°-dominate laminates but reduced strengths of 90°-dominated laminates by approximately 10%. Differing intraply hybridization architectures resulted in differing damage progression and distinct sensitivities to changes in notch length.

Classical methods of correcting for finite specimen width were found to underpredict actual width effects for relatively benign specimen geometries. This confirmed earlier

findings for more severe configurations and indicates that the stress/strain distributions within the coupons do not conform to the assumptions of the classical methods. Similar problems are expected when trying to quantify structural configuration factors. This has important considerations relating to efforts to standardize material screening tests and structural scaling laws. An understanding of the effects of specimen geometry and interactions with material type and laminate layup are essential to optimal material selection and structural design.

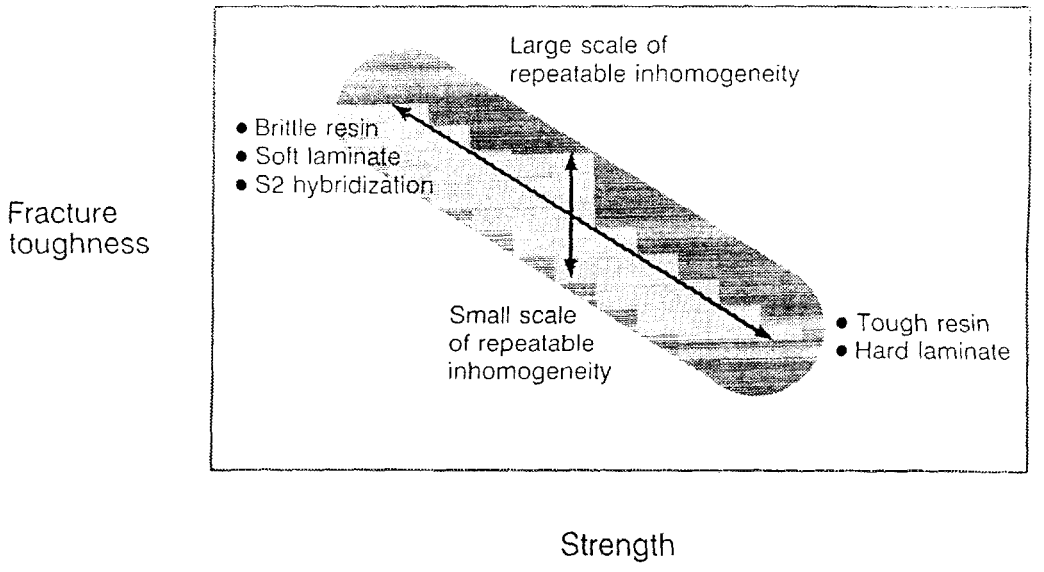

Figure 32. Strength-toughness trade-off in composite materials.

Classical fracture strength models were found to be inaccurate for predicting the large-notch strengths of four of the five laminate/material combinations tested. Measured pre-damage crack-tip strain distributions were significantly higher than assumed in classical methods for the same four laminate/material combinations. The exception in both cases was a 0°-dominate laminate fabricated from IM7/8551-7. The higher strains may result in (a) finite width effects that are stronger than expected and (b) inaccurate strength predictions. The Mar-Lin method was found to predict the large-notch strengths from small notch results through the use of a reduced stress-field singularity. Variations in the singularity modeled the differing sensitivities to changes in notch lengths observed in the test results.

Two stiffened panel fracture tests, each with a severed skin-bay and stiffening element, were conducted. The panel fabricated from AS4/938 exhibited a strength approximately 23% below that of an identical panel fabricated from an intraply hybrid of 25% S2/938 and 75% AS4/938. Skin fracture controlled the final failure of both panels, with load redistribution to the intact stiffening elements significantly affecting the damage growth prior to failure. Strain softening models were identified as attractive for addressing the global load redistribution effects of local damage progression.

REFERENCES

1. Ilcewicz, L. B., Smith, P. J., and Horton, R. E., "Advanced Composite Fuselage Technology," *3rd NASA Advanced Composites Technology Conference*, NASA CP-3178.

2. Smith, P. J., Koch, W. J., Bodine, J. B., and Preuss, C. H., "Design, Analysis, and Fabrication of a Pressure Box Test Fixture for Tension Damage Tolerance Testing of Curved Fuselage Panels," *3rd NASA Advanced Composites Technology Conference*, NASA CP-3178.

3. Walker, T. H., Avery, W. B., Ilcewicz, L. I., Poe, C. C., Jr., and Harris, C. E., "Tension Fracture of Laminates for Transport Fuselage - Part I: Material Screening," *Second NASA Advanced Technology Conference*, NASA CP 3154, pp. 197-238, 1991.

4. Broek, D., *The Practical Use of Fracture Mechanics*, Kluwer Academic Publisher, 1989.

5. Chang, J. B., and Rudd, J. L. (eds.), *Damage Tolerance of Metallic Structures: Analysis Methods and Applications*, ASTM STP 842, 1984.

6. Willden, K., Metschan, S., Grant, C., and Brown, T., "Composite Fuselage Crown Panel Manufacturing Technology," *Second NASA Advanced Technology Conference*, NASA CP 3154, pp. 263-291, 1991.

7. Poe, C. C., Jr., and Kennedy, J. M., "An Assessment of Buffer Strips for Improving Damage Tolerance of Composite Laminates," *J. of Composite Materials Supplement*, Vol. 14, pp. 57-70, 1980.

8. Kennedy, J. M., "Damage Tolerance of Woven Graphite/Epoxy Buffer Strip Panels," NASA TM 102702, 1990.

9. Swift, T., "Damage Tolerance in Pressurized Fuselages," *14th Symposium of the International Committee on Aeronautical Fatigue - New Materials and Fatigue Resistant Aircraft Design*, 1987.

10. Awerbuch, J., and Madhukar, M. S., "Notched Strength of Composite Laminates: Predictions and Experiments -- A Review," *J. of Reinforced Plastics and Composites*, Vol. 4, pp. 1-159, 1985.

11. Konish, H. J., Jr., "Mode I Stress Intensity Factors for Symmetrically-Cracked Orthotropic Strips," in *Fracture Mechanics of Composites*, ASTM STP 593, American Society for Testing and Materials, pp. 99-116, 1975.

12. Poe, C. C., Jr., and Sova, J. A., "Fracture Toughness of Boron/Aluminum Laminates with Various Proportions of 0° and ±45° Plies," NASA Technical Paper 1707, 1980.

13. Cairns, D., Walker, T., and Ilcewicz, L., "Response of Automated Tow Placed Laminates to Stress Concentrations," *3rd NASA Advanced Composites Technology Conference*, NASA CP-3178.

14. Nakamura, S., and Lakes, R. S., "Finite Element Analysis of Stress Concentration Around a Blunt Crack in a Cosserat Elastic Solid," *Computer Methods in Applied Mechanics and Engineering*, Vol. 66, pp. 257-266, 1988.

15. Nakamura, S. Benedict, R., and Lakes, R. S., "Finite Element Method for Plane Micropolar Elasticity," *International Journal of Engineering Sciences*, Vol. 22, pp. 319-330, 1984.

16. Chong, W., and Zhi-Da, C., "Microroation Effects in Material Fracture and Damage," *Engineering Fracture Mechanics*, Vol. 38, No. 2/3, pp. 147-155, 1991.

17. Chang, F. K., and Chang, K. Y., "A Progressive Damage Model for Laminated Composites Containing Stress Concentrations," J. of Composite Materials, Vol. 32, pp. 834-855, 1987.

18. Mazars, J. and Bazant, Z. P. (eds.), *Crackin And Damage: Strain Localization and Size Effect*, Elsevier Applied Science, 1988.

19. Llorca, J., and Elices, M., "A Cohesive Crack Model to Study the Fracture Behaviour of Fiber-Reinforced Brittle-Matrix Composites," *International Journal of Fracture*, Vol. 54, pp. 251-267, 1992.